Journal of ELECTRONIC MATERIALS, Vol. 39, No. 3, 2010
DOI: 10.1007/s11664-009-1061-3

Measurements of Microhardness and Thermal and Electrical Properties of the Binary Zn-0.7wt.%Cu Hypoperitectic Alloy

H. KAYA,[1,5] U. BÖYÜK,[1] S. ENGİN,[2] E. ÇADIRLI,[3] and N. MARAŞLI[4]

1.—Department of Science Education, Faculty of Education, Erciyes University, 38039 Kayseri, Turkey. 2.—Department of Physics, Institute of Science and Technology, Erciyes University, 38039 Kayseri, Turkey. 3.—Department of Physics, Faculty of Arts and Sciences, Niğde University, 51200 Nigde, Turkey. 4.—Department of Physics, Faculty of Arts and Sciences, Erciyes University, 38039 Kayseri, Turkey. 5.—e-mail: hasankaya@erciyes.edu.tr

Zn-0.7wt.%Cu hypoperitectic alloys were directionally solidified upwards with different temperature gradients (3.85 K/mm to 9.95 K/mm) at a constant growth rate (0.042 mm/s), and with different growth rates (0.0083 mm/s to 0.436 mm/s) at a constant temperature gradient (3.85 K/mm), using a Bridgman-type growth apparatus. Measurements of microhardness of the directionally solidified samples were carried out. The dependence of microhardness (HV) on growth rate (V) and temperature gradient (G) was analyzed. According to these results, it has been found that, for increasing values of G and V, the value of HV increases. Variations of electrical resistivity (ρ) and electrical conductivity (σ) for cast samples with temperature from 300 K to 670 K were also measured by using a standard direct-current (DC) four-point probe technique. The variation of the Lorenz coefficient with temperature for the Zn-0.7wt.%Cu hypoperitectic alloy was determined using the measured values of electrical conductivity and thermal conductivity. The enthalpy of fusion for the same alloy was determined by means of differential scanning calorimetry (DSC) from the heating trace during the transformation from liquid to solid.

Key words: Zn-Cu alloy, cellular microstructure, microhardness, electrical conductivity, Lorenz coefficient, enthalpy, specific heat

INTRODUCTION

Zinc-based alloys have high strength and hardness, so they are ideal alternatives to machined, pressed, stamped, and fabricated items. Complex net-shaped zinc housings with precise thin walls provide excellent electrical performance and shielding properties for electronic connectors as well as shields, chassis, and frames for handheld telecommunication and computing equipment. Zinc-based alloys have been used in many applications, including mobile-phone antennae, portable computers, disk drives, radiofrequency circuits, transformer cores, high-quality filters, precision interlocking gears, heat sinks, shutter mechanisms in cameras, and many other electrical and electronics consumer applications.[1–3] Moreover, the mechanical properties of zinc-based alloys make them attractive substitutes for cast iron and copper alloys in many structural and pressure-tight applications. Because zinc is less costly than copper, these zinc-based alloys have a distinct cost advantage over copper-based alloys.[4–8]

Peritectic alloys occupy an outstanding position among engineering materials. Many technically important alloy systems such as steels, Cu alloys, rare-earth permanent magnets, and high-T_c superconductors display peritectic reactions where phase and microstructure selection play an important role in the processing and properties of the material.[9–11]

Peritectic microstructures are characterized by growth competition between a primary η phase and a peritectic ε phase, which can both coexist with the liquid at the peritectic temperature T_p (Fig. 1). When the peritectic alloy directionally solidifies

(Received August 6, 2009; accepted December 14, 2009; published online January 20, 2010)

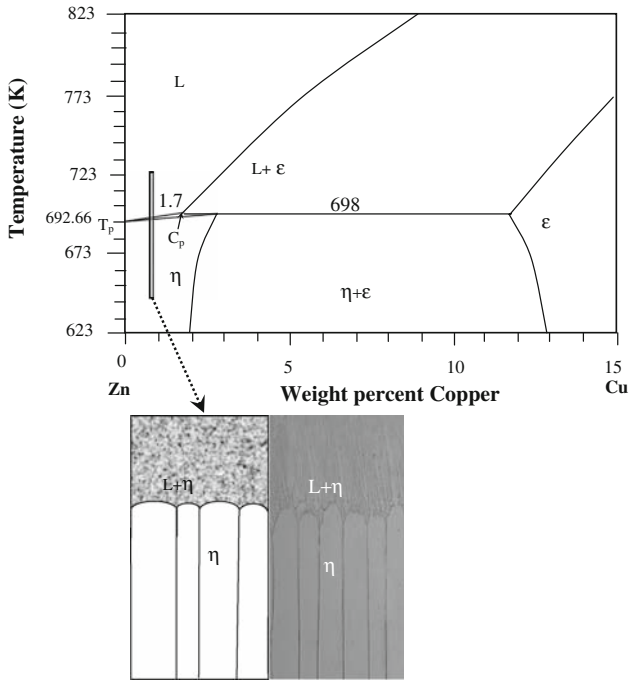

Fig. 1. A partial phase diagram of the Zn-Cu system (after Ref. 15) and the microstructures of directionally solidified Zn-0.7wt.%Cu alloy.

under planar growth conditions, the rejection of solute in the liquid leads to the formation of a solute boundary layer.[12] The composition in the liquid at the interface increases as the single phase solidifies, and the interface temperature decreases until the steady-state growth condition is achieved at the solidus temperature of the alloy. The three-phase peritectic reaction, liquid + solid (ε) $\rightarrow$ solid (η), cannot occur at the peritectic temperature (T_p) but must occur below T_p.[12]

In peritectic systems, two-phase morphologies have been observed under conditions close to the limit of constitutional undercooling, such as peritectic banding, oscillation, and peritectic coupled growth.[13–15] Simultaneous (coupled) growth of two phases with planar solid–liquid interface has been suggested to occur in peritectic alloys close to the peritectic temperature, similar to in eutectic alloys.[16] Coupled growth is characterized by a macroscopically composite front in which the two phases grow together parallel to the growth direction with either lamellar or rod morphology. Cellular peritectic coupled growth is only possible when both phases are morphologically stable and the liquid between the cells becomes richer in Cu atoms.[17]

Zn-Cu alloys, which are typical peritectic alloys with cellular structure, have recently attracted much attention. Therefore, the Zn-rich Zn-0.7wt.%Cu alloy system was selected as a model system to investigate the cellular structure in peritectic alloys. The Zn-Cu alloys are an excellent alloy system to study coupled growth, for three main reasons: firstly, Zn-Cu alloys are typical binary peritectic systems in which four peritectic reactions occur over the whole composition range; secondly, in contrast to many other peritectic systems, the mushy zone range is small ($\sim$3 K), which makes it convenient to carry out experiments (Fig. 1); and thirdly, all necessary physical parameters related to the Zn-Cu system are well known.

Thus, the purposes of the present work are to study the dependency of microhardness on the solidification processing parameters (G and V) and microstructures (cellular spacing, λ, and cell tip radius, R) for directionally solidified Zn-0.7wt.%Cu hypoperitectic alloy and also to investigate the dependency of electrical resistivity (ρ) and electrical conductivity (σ) of Zn-0.7wt.%Cu cast samples on temperature in the range of 300 K to 670 K. Besides, the variation of the Lorenz coefficient with temperature for Zn-0.7wt.%Cu alloy was determined by using the measured values of electrical conductivity and thermal conductivity. The enthalpy of fusion and the specific heat for the same alloy were determined from the DSC curve.

EXPERIMENTAL PROCEDURE

Sample Preparation and Solidification

Using vacuum melting and hot-filling furnaces, Zn-0.7wt.%Cu alloy was prepared under vacuum by using 99.99% purity zinc and copper. After allowing time for melt homogenization, the molten alloy was poured into 13 graphite crucibles (200 mm length, 4 mm ID, 6.35 mm OD) held in a specially constructed sample hot-filling furnace at approximately 50 K above the melting point of the alloy. The molten alloy was directionally solidified from bottom to top to ensure that the crucible was completely full.

Solidification of the samples was carried out with different temperature gradients (3.85 K/mm to 9.95 K/mm) at a constant growth rate (0.042 mm/s), and with different growth rates (0.0083 mm/s to 0.436 mm/s) at a constant temperature gradient (3.85 K/mm), in a Bridgman-type growth apparatus. The temperature of the water in the reservoir was kept at 283 K to an accuracy of $\pm$0.1 K using a Poly Science digital 9102 model heating/refrigerating circulating bath, to obtain a well-quenched solid–liquid interface. The temperature on the sample was also controlled to an accuracy of $\pm$0.1 K by using a Eurotherm 2604 type controller. More details of the apparatus and experimental procedures are given in Ref. 18.

Measurements of Temperature Gradient and Growth Rate

The temperature in the specimen was measured by using three K-type 0.25-mm-diameter insulated thermocouples fixed within the sample with spacing of 10–20 mm. In the present work, a 1.2 mm OD $\times$ 0.8 mm ID alumina tube was used to insulate

Table I. Solidification processing parameters, microstructures, and microhardness for directionally solidified Zn-0.7wt.%Cu alloy, and relationships between them

Solidification Parameters		Microstructures and Microhardness				
G (K/mm)	V (mm/s)	λ_T ($\times 10^{-2}$ mm)	λ_L ($\times 10^{-2}$ mm)	R ($\times 10^{-2}$ mm)	HV_T (kg/mm^2)	HV_L (kg/mm^2)
3.85	0.042	9.89 ± 055	8.32 ± 0.50	1.62 ± 0.164	55.90 ± 3.04	52.60 ± 2.61
5.54	0.042	7.60 ± 0.56	6.79 ± 0.44	1.48 ± 0.15	57.40 ± 2.70	54.00 ± 2.60
7.57	0.042	6.49 ± 0.32	5.57 ± 0.31	1.26 ± 0.13	60.60 ± 2.54	57.30 ± 2.51
8.18	0.042	6.18 ± 0.32	5.29 ± 0.28	1.14 ± 0.11	61.50 ± 2.73	58.50 ± 2.66
9.95	0.042	5.68 ± 0.29	4.97 ± 0.25	1.03 ± 0.09	63.50 ± 2.91	60.00 ± 2.72
3.85	**0.008**	14.71 ± 0.61	11.09 ± 0.632	3.01 ± 0.17	53.10 ± 3.30	49.20 ± 2.70
3.85	**0.016**	12.51 ± 0.66	10.58 ± 0.560	2.65 ± 0.16	54.50 ± 3.11	50.80 ± 2.55
3.85	**0.042**	9.89 ± 0.55	8.32 ± 0.50	1.61 ± 0.16	55.90 ± 3.04	52.60 ± 2.61
3.85	**0.830**	8.53 ± 0.41	7.04 ± 0.37	1.12 ± 0.12	59.00 ± 3.22	55.70 ± 2.74
3.85	**0.144**	7.14 ± 0.29	5.51 ± 0.17	0.87 ± 0.08	65.00 ± 2.42	61.40 ± 2.33
3.85	**0.436**	5.07 ± 0.13	4.35 ± 0.14	0.40 ± 0.05	66.30 ± 2.10	63.10 ± 3.01

Relationships	Constants (k)	Correlation Coefficients (r)
$HV_T = k_1 G^{0.14}$	$k_1 = 46.03\ K^{-0.14}\ kg\ mm^{-1.86}$	$r_1 = 0.984$
$HV_L = k_2 G^{0.15}$	$k_2 = 47.74\ K^{-0.15}\ kg\ mm^{-1.85}$	$r_2 = 0.982$
$HV_T = k_3 V^{0.07}$	$k_3 = 70.15\ kg\ mm^{-2.07}\ s^{0.07}$	$r_3 = 0.958$
$HV_L = k_4 V^{0.08}$	$k_4 = 67.14\ kg\ mm^{-2.08}\ s^{0.08}$	$r_4 = 0.969$
$HV_T = k_5(\lambda_T)^{-0.23}$	$k_5 = 35.81\ kg\ mm^{-1.77}$	$r_5 = -0.975$
$HV_L = k_6(\lambda_L)^{-0.25}$	$k_6 = 28.44\ kg\ mm^{-1.75}$	$r_6 = -0.978$
$HV_L = k_7(R)^{-0.46}$	$k_7 = 46.23\ kg\ mm^{-1.54}$	$r_7 = -0.520$

λ_T, average cellular spacing measured from transverse section; λ_L, average cellular spacing measured from longitudinal section; HV_L, microhardness obtained from longitudinal section; HV_T, microhardness obtained from transverse section; R, cell tip radius measured from longitudinal section.
Bold values in the G column show change of the gradient values. Bold values in the V column show changes of the growth rate values.

the thermocouples from the melt. All the thermocouples' ends were then connected to a measurement unit consisting of a data-logger and a computer. The cooling rates were recorded by using the data-logger via the computer during growth. When the solid–liquid interface was at the second thermocouple, the temperature difference between the first and second thermocouples (ΔT) was read from the data-logger record. The temperature gradient in the liquid phase for each sample was determined using the measured values of ΔT and ΔX.

The time taken for the solid–liquid interface to pass the thermocouples separated by known distances was read from the data-logger record. Thus, the growth rate for each sample was determined using the measured value of ΔT and known value of ΔX. The calculated values of G and V are given in Table I.

Metallographic Analysis

The quenched samples were removed from the graphite crucible, and 3-cm lengths from the top and bottom were cropped off and discarded. Then the rest of the samples were ground to observe the solid–liquid interface, and the longitudinal section including the quenched interface was separated from the specimen. This part was ground, polished, and etched to reveal the quenched interface. Furthermore, the ground specimens were mounted in a cold-setting epoxy resin. The longitudinal and transverse sections were wet-ground down to 2500 grit and mechanically polished using 6-μm, 3-μm, 1-μm, and 0.25-μm diamond pastes. Finally, the specimens were etched in a solution (20 g CrO_3 plus 3 g Na_2SO_4 in 100 mL distilled water) for 15 s. Following the metallographic preparation, the microstructures of the samples were revealed. The microstructures of samples were characterized from both transverse and longitudinal sections of samples using an Olympus BX-51 optical microscope. Typical images of growth morphologies of the directionally solidified Zn-0.7wt.%Cu peritectic alloy are shown in Fig. 2, showing that the microstructures were of cellular form.

Measurement of Cellular Spacing

The cellular spacing measured from the longitudinal section, λ_L, was obtained by measuring the distance between the nearest two cell centers (Fig. 2a). Two different methods were used for measurement of the cellular spacing (λ_T) on the transverse sections (Fig. 2b). The first method is the triangle method.[19] A triangle is formed by joining the three neighboring cell centers, and the sides of

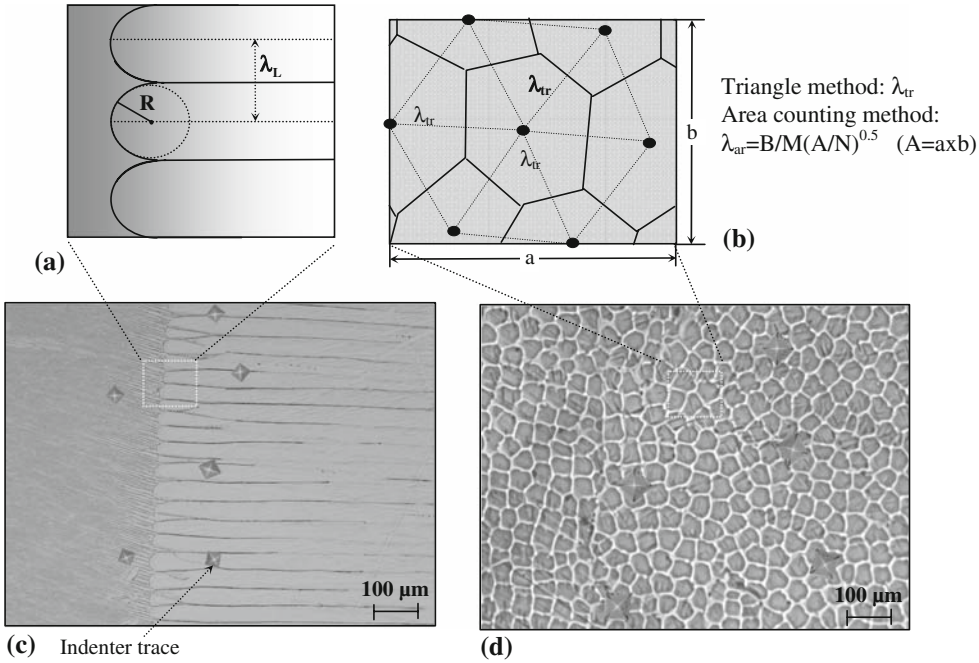

Fig. 2. Schematic illustration of the cellular spacing measurements on: (a) longitudinal section, and (b) transverse section. Cellular microstructure of the directionally solidified Zn-0.7wt.%Cu alloy: (c) longitudinal section, and (d) transverse section (G = 9.95 K/mm, V = 0.042 mm/s).

the triangle correspond to λ_{tr} (Fig. 2b). Using this method, at least 30 to 40 cellular spacing were measured for each sample. The second method is the area counting method (Fig. 2b).[20] In this method, the cellular spacing values, λ_{ar}, were calculated from:

$$\lambda_{ar} = \frac{B}{M}\left(\frac{A}{N}\right)^{0.5}, \qquad (1)$$

where B (1.075 for hexagonal structures) is the correction factor, M is the magnification factor, A is the total specimen cross-section area, and N is the number of cells on the cross-section. λ_{ar} values were measured on the transverse section for at least five different regions for each specimen using this method. The value of λ_T is the average of λ_{ar} and λ_{tr}, as given in Table I.

The cell tip radius defined in Fig. 2a, was measured by fitting a suitable circle to the cell tip side. These measurements were repeated at least 20 to 30 times on the cells for each G and V.

Measurement of Microhardness

One of the purposes of this investigation is to obtain the relationships among solidification processing parameters (G and V) and microhardness (HV) for the directionally solidified Zn-0.7wt.%Cu alloy. The mechanical properties of any solidified material are usually determined by hardness test, tensile test, etc. Since true tensile strength testing of solidified alloys gave inconsistent results with a wide scatter due to the strong dependence on solidified sample surface quality, the mechanical properties were monitored by hardness testing, which is one of the easiest and most straightforward techniques. Microhardness measurements in this work were carried out using a Future-Tech FM-700 hardness measuring test device using a 10 g to 50 g load and a dwell time of 10 s, giving a typical indentation depth of about 40 μm to 60 μm, which is significantly smaller than the original solidified samples. Microhardness was measured for at least 20 different regions on transverse, HV_T, and longitudinal sections, HV_L. The measured values of G, V, and HV are also given in Table I, and the variations of microhardness with the solidification processing (G and V) and microstructure parameters (λ and R) are plotted in Figs. 3 and 4.

Measurement of Electrical Resistivity and Electrical Conductivity

The dependence of the electrical resistivity (ρ) and electrical conductivity (σ) on temperature for casting of Zn-0.7wt.%Cu alloy was measured by the DC four-point probe method. The four-point probe method is the most widely used technique for electrical profile measurement of materials. The method has proven to be a convenient tool for resistivity measurement. A four-point probe measurement is performed by making four electrical contacts to a sample surface. The specimen thickness and width were measured to an accuracy of 1 μm using a digital micrometer. The resistance data were converted to resistivity values by using the measured specimen dimensions.

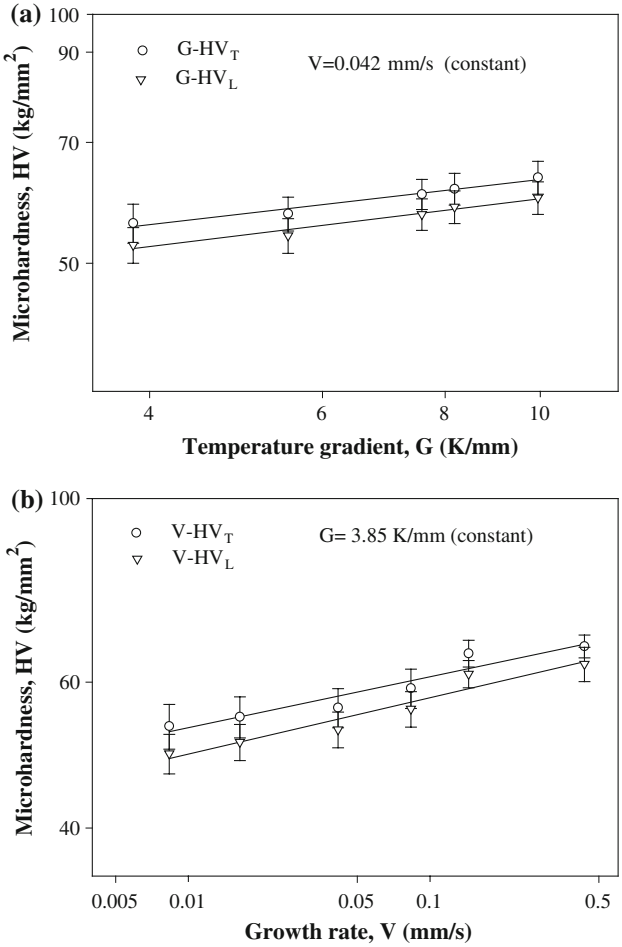

Fig. 3. Variation of microhardness with (a) the temperature gradient and (b) the growth rate.

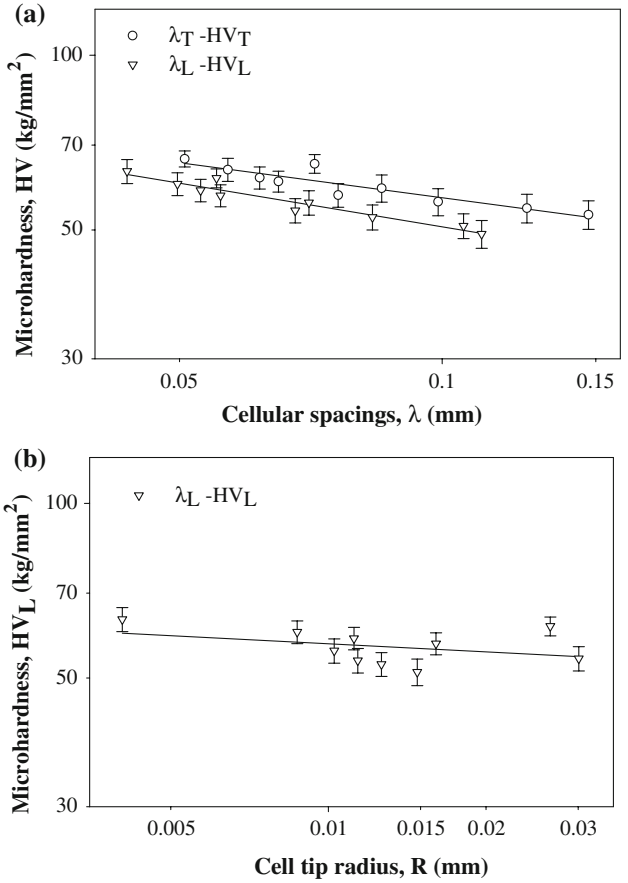

Fig. 4. Variation of microhardness with (a) the cellular spacing and (b) the cell tip radius.

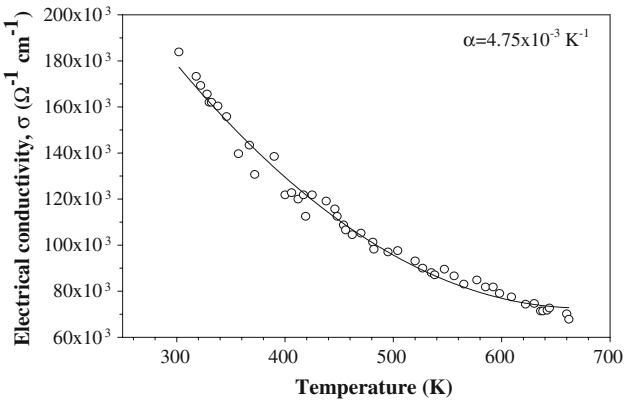

Fig. 5. Dependence of electrical conductivity on temperature.

Electrical resistivity strongly depends on temperature. In metals, electrical resistivity increases with increasing temperature. The dependence of electrical resistivity on temperature is often expressed as the slope of the graph of electrical resistivity or conductivity versus temperature and can be given as

$$\alpha = \frac{\rho_S - \rho_0}{\rho_0(T - T_0)} = \frac{1}{\rho_0}\frac{\Delta\rho}{\Delta T}, \quad (2)$$

where ρ_S is the electrical resistivity at temperature T, ρ_0 is the electrical resistivity at room temperature, T_0 = 300 K, and α is the temperature coefficient of resistivity.

The temperature dependence of the electrical conductivity for the Zn-0.7wt.%Cu cast samples are given in Fig. 5. The electrical conductivity of cast samples is inversely proportional to temperature.

Determination of Enthalpy and Specific Heat

The enthalpy of fusion (ΔH) and the specific heat (C_p) of Zn-0.7wt.%Cu hypoperitectic alloy were determined because they are very important parameters for industrial applications. DSC thermal analysis (Perkin Elmer Diamond model) was performed in the temperature range from 300 K to 720 K at a heating rate of 10 K/min under a constant stream of nitrogen at atmospheric pressure.

We used a reference material (a sapphire disk) in determining specific heat. This reference data is used to "correct" sample data at every temperature. The size of the signal from which the specific heat is calculated is proportional to the heating rate used,

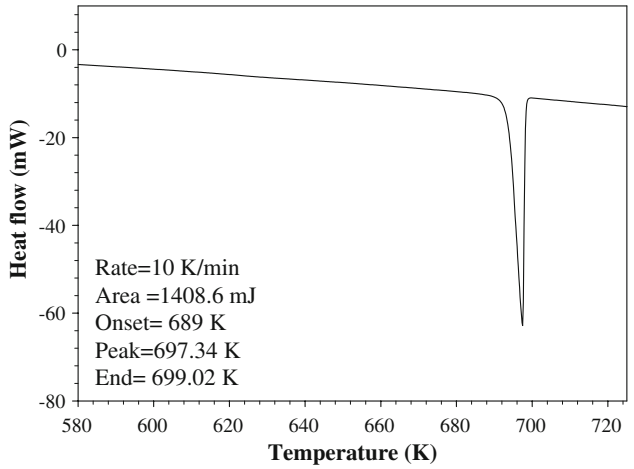

Fig. 6. Heat flow versus temperature for Zn-0.7wt.%Cu alloy at heating rate of 10 K/min.

so it follows that faster heating rates will produce larger signals, which would give more accurate data. However, if the heating rate is too high, the temperature gradients in the sample will be large and this may introduce other errors in the measurement. It is normal to use heating rates between 5 °C/min and 20 °C/min. The heating rate in this study was 10 °C/min, which is mostly recommended.

The difference between the sample curve and the baseline curve is measured in milliwatts and converted to specific heat as follows,[21]

$$C_p = \frac{dQ}{dt}\frac{1}{m\beta}, \tag{3}$$

where dQ/dt is the heat flow, m is the mass of the sample, and β is the heating rate in °C/min.

The DSC curve obtained for Zn-0.7wt.%Cu hypoperitectic alloy is shown in Fig. 6. A sharp peak is clearly observed for the melting process, as shown in Fig. 6. The enthalpy of fusion (ΔH) and specific heat (C_p) were calculated as the area under the peak by numerical integration.

Measurement of Thermal the Conductivity

Thermal conductivity of the solid Zn-based Zn-Cu alloy was measured by using a radial heat flow apparatus. The radial heat flow method is an ideal technique for measuring the thermal conductivity of solid phases. In the steady-state condition, the temperature gradient in the cylindrical specimen is given by Fourier's law

$$\frac{dT}{dr} = -\frac{Q}{AK_s}, \tag{4}$$

where Q is the total input power from the center of the specimen, A is the surface area of the specimen, and K_s is the thermal conductivity of the solid phase. Integration of Eq. 4 gives

$$K_s = a_0\frac{Q}{T_1 - T_2}, \tag{5}$$

where $a_0 = \ln(r_2/r_1)/2\pi l$ is an experimental constant, r_1 and r_2 ($r_2 > r_1$) are fixed distances from the center axis of the specimen, l is the constant length of the heating wire, and T_1 and T_2 are the temperatures at the fixed positions, r_1 and r_2. Equation 5 can be used to obtain the thermal conductivity of the solid phase by measuring the temperature difference between the two fixed points for a given power level provided that the vertical temperature variations are minimum or zero. The details of the apparatus and experimental procedures are given in Ref. 22.

RESULTS AND DISCUSSION

Dependence of Microhardness on Solidification and Microstructure Parameters

As can be seen from Table I and Fig. 3a, the dependence of microhardness on G was determined by using linear regression analysis and the relationship between them can be expressed as

$$HV = k_1 G^a, \tag{6}$$

where k_1 is a constant and a is the exponent value relating to the temperature gradient. The values of the exponent relating to the temperature gradient were obtained as 0.14 and 0.15 for the transverse and longitudinal sections, respectively. These exponent values are very close to the values of 0.17 and 0.14 obtained by Kaya et al.[23] for cellular growth of Al-0.1wt.%Ti and Al-2wt.%Li alloys under similar solidification conditions, respectively.

Variations of the values of HV as a function of V at constant G are given in Table I and Fig. 3b. As can be seen from Table I and Fig. 3b the dependence of HV on V can be represented as

$$HV = k_2 V^b. \tag{7}$$

The exponent values of V were obtained as 0.07 and 0.08 for the transverse and longitudinal sections, respectively. These exponent values are in good agreement with the exponent values of V (0.06 to 0.10) obtained by various researchers[23–26] for different alloy systems.

The variations of microhardness as a function of cellular spacing and cell tip radius are given in Table I and Fig. 4a. It can be observed that a decrease in cellular spacing and cell tip radius leads to an increase in HV. Linear regression analysis yields

$$HV = k_3(\lambda)^{-c}, \tag{8a}$$

$$HV = k_4(R)^{-d}. \tag{8b}$$

The exponent values of λ were obtained as 0.23 and 0.25 for the transverse and longitudinal sections,

respectively. Also, the exponent value of R was obtained as 0.46 for the longitudinal section.

These exponent values relating to the cellular spacings are in good agreement with the exponent values of λ (0.20 to 0.28) obtained by different researchers[23–26] for cellular and eutectic growth. However, the exponent values of λ obtained in this work are smaller than the values of 0.50 and 0.50 obtained by Telli and Kısakürek[27] and by Al-Si and Lapin et al.[28] for the Ti-46Al-2W-15Si alloy system, respectively. These differences in the exponent values might be due to different alloy compositions, different microstructures, and different solidification conditions.

Electrical Properties of Zn-0.7wt.%Cu Alloy

As mentioned above, the variation of electrical resistivity (ρ) with temperature in the range from 300 K to 670 K for Zn-0.7wt.%Cu alloy was measured. The values of ρ were found to be in the range from 5.43×10^{-6} Ω cm to 14.75×10^{-6} Ω cm. The values of ρ are very close to the values of 11.14×10^{-6} Ω cm, 13.05×10^{-6} Ω cm, and 15.68×10^{-6} Ω cm obtained by El-Ashram and Shalaby[29] for the similar alloys of Sn-0.7wt.%Cu, Sn-0.7wt.%Cu-0.5wt.%Zn, and Sn-0.7wt.%Cu-0.5wt.%Bi, respectively. Also, the values of ρ in the present work are very close to the values of 11.5×10^{-6} Ω cm and 15.8×10^{-6} Ω cm obtained by Saatci et al.[30] for the Cd-5at.%Zn and Zn-1.3at.%Cd alloy systems, respectively.

As can be seen from Fig. 5, σ is inversely proportional to temperature and found to be in the range of 183×10^{3} Ω^{-1} cm^{-1} to 68×10^{3} Ω^{-1} cm^{-1}. The temperature coefficient of electrical resistivity for Zn-0.7wt.%Cu alloy was determined to be 4.75×10^{-3} K^{-1} from the graph of electrical resistivity variation versus temperature.

Thermal Properties of Zn-0.7wt.%Cu Alloy

Variation of the thermal conductivity (K_s) of the solid phase for Zn-0.7wt.%Cu alloy with temperature was measured by Kaygısız et al.[22] and is shown in Fig. 7. The thermal conductivity is slightly decreasing with increasing temperature in the range of 350 K to 700 K. The value of K_s for Zn-0.7wt.%Cu alloy at the melting temperature was obtained as 141.81 W/K m by extrapolating to the peritectic temperature.[22]

The electrical conductivity is a measure of a material's ability to conduct an electric current and is one of the important physical material properties along with thermal conductivity, specific heat, and thermal expansion. The relationship between the thermal conductivity and the electrical conductivity is established by the Wiedemann–Franz law, which is based upon the fact that heat and electrical transport both involve the free electrons in the metal, as

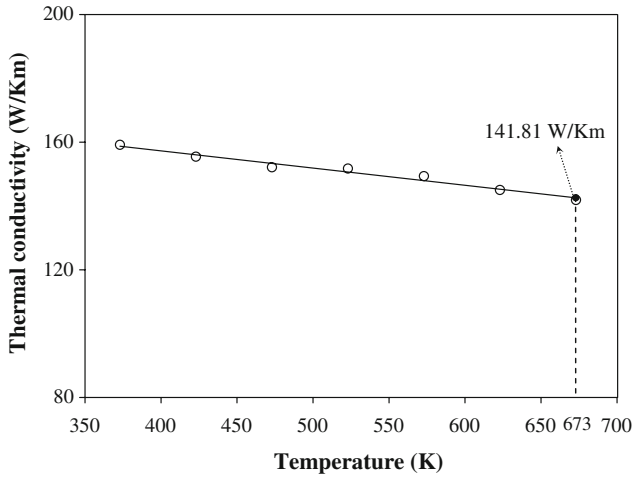

Fig. 7. Thermal conductivity of solid Zn-0.7wt.%Cu alloy versus temperature.[22]

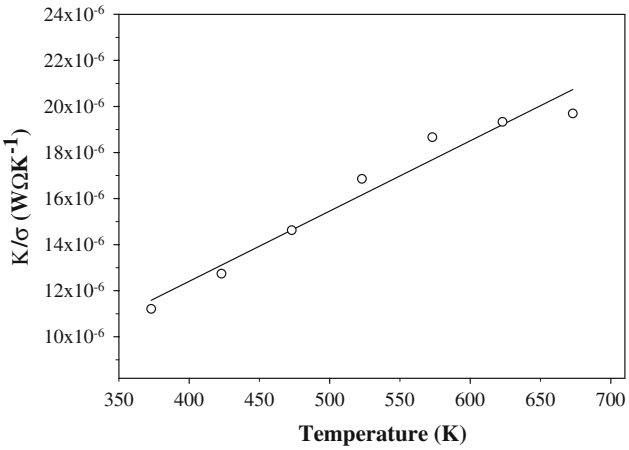

Fig. 8. The values of K/σ versus temperature.

$$\frac{K_s}{\sigma} = LT, \tag{9}$$

where L is the constant of proportionality (2.45×10^{-8} W Ω K^{-2}), which is called the Lorenz number.[31]

The ratio of the thermal conductivity to the electrical conductivity for Zn-0.7wt.%Cu alloy as a function of temperature was determined from Figs. 5 and 7 and is plotted in Fig. 8. The value of the Lorenz number for Zn-0.7wt.%Cu alloy was determined from Eq. 6 as a function of temperature and is given in Table II. The result also shows that the Lorenz number increases slightly with increasing temperature. The Lorenz number, L, is 2.88×10^{-8} W Ω K^{-2} at 373 K. The L value in the present work is in good agreement with the values of 2.97×10^{-8} W Ω K^{-2} and 2.70×10^{-8} W Ω K^{-2} obtained by Saatci et al.[31] for the Cd-5at.%Zn and Zn-1.3at.%Cd alloy systems at 373 K, respectively.

Table II. Lorenz number as a function of temperature for Zn-0.7wt.%Cu alloy

Temperature, T (K)	Lorenz Number ($\times 10^{-8}$), L (W Ω K^{-2})
373	2.88
423	3.06
473	3.22
523	3.30
573	3.38
623	3.47
673	3.51

As can be seen from Table II, experimental L values deviate from the Wiedemann–Franz law. This discrepancy can be interpreted as indicating that some other mechanism, such as electron–electron interaction, phonon–phonon interaction, grain boundary/impurity scattering etc., are involved in the thermal conduction process.

The Zn-0.7wt.%Cu alloy was heated at a heating rate of 10 K/min from room temperature to 720 K by using a Perkin Elmer Diamond DCS device, and the resulting heat flow versus temperature curve for Zn-0.7wt.%Cu alloy is shown in Fig. 6. As can be seen from Fig. 6, the melting temperature of Zn-0.7wt.%Cu alloy was detected to be 697.34 K. The values of the enthalpy of fusion (ΔH) and the specific heat (C_p) for Zn-0.7wt.%Cu alloy were also calculated to be 159.12 J/g, and 0.375 J/g K, respectively, from the graph of heat flow versus temperature. The recommended values of the enthalpy of fusion (ΔH) and the specific heat (C_p) for pure Zn are 112.0 J/g and 0.54 J/g K, respectively,[32] at the melting temperature (692 K).

CONCLUSIONS

The principal results in this work can be summarized as follows.

The values of HV for directionally solidified Zn-0.7wt.%Cu alloy have been measured on the transverse section as well as on the longitudinal sections. It was found that the microhardness increases with increasing G and V as well as with decreasing λ and R. Thus, the value of HV can be increased by increasing the value of the cooling rate ($G{\cdot}V$).

The electrical resistivity (ρ) of Zn-0.7wt.%Cu alloy increased with increasing temperature as the electrical conductivity (σ) decreased.

Variation of the Lorenz number with temperature for the Zn-0.7wt.%Cu hypoperitectic alloy was obtained from the experimental K/σ values as a function of temperature. The Lorenz number slightly deviated from the Wiedemann–Franz law.

The Zn-0.7wt.%Cu alloy was heated at a rate of 10 K/min from 580 K to 720 K. From the plot of heat flow versus temperature, the melting temperature, the enthalpy of fusion (ΔH), and the specific heat (C_p) for Zn-0.7wt.%Cu alloy were found to be 697.34 K, 159.12 J/g, and 0.375 J/g K, respectively.

ACKNOWLEDGEMENTS

This research was supported financially by the Scientific and Technical Research Council of Turkey (TUBİTAK) under Contract No. 107T095. The authors are grateful to the Scientific and Technical Research Council of Turkey (TUBİTAK) for their financial support.

REFERENCES

1. W. Cubberly and R. Bakerjian, *Tool and Manufacturing Engineers Handbook*, Desk Edition (Dearborn, MI: Society of Manufacturing Engineers, 1989), pp. c15, 40–41.
2. H.S. Park, T. Kimura, T. Murakami, Y. Nagano, K. Nakata, and M. Ushio, *Mater. Sci. Eng. A* 371, 160 (2004).
3. O.V. Flores, C. Kennedy, L.E. Murr, D. Brown, S. Pappu, B.M. Nowak, and J.C. McClure, *Scripta Mater.* 38, 703 (1998).
4. T. Hashimoto, S. Jyogan, K. Nakata, Y.G. Kim, and M. Ushio, *Proceedings of the 1st International Symposium on Friction Stir Welding* (Thousand Oaks, CA, USA: Rockwell Science Center, 14–16 June 1999).
5. C.G. Andersson, R.E. Andrews, B.G.I. Dance, M.J. Russel, E.J. Olden, and R.M. Sanderson, *Proceedings of the 2nd FSW Symposium on Comparison of Copper Canister Fabrication by the Electron Beam and Friction Stir Processes* (Gothenburg, Sweden, 26–28 June 2000).
6. K.S. Bang, W.B. Lee, Y.M. Yeon, and S.B. Jung, *International Welding/Joining Conference-Korea 2002* (Gyeongju, Korea, 28–30 October 2002).
7. P. Ravindranathan and K.C. Patal, *Mater. Sci.* 22, 3261 (1987).
8. F.Y. Hung, T.S. Lui, L.H. Chen, and J.G. You, *J. Mater. Sci.* 42, 3865 (2007).
9. D.A. Porter and K.E. Easterling, *Phase Transformations in Metals and Alloys*, 2nd ed. (CRC Press, 1992), p. 185.
10. O. Hunziker, M. Vandyoussefi, and W. Kurz, *Acta Mater.* 46, 6325 (1998).
11. H.W. Kerr and W. Kurz, *Int. Mater. Rev.* 41, 129 (1996).
12. R. Trivedi and J.S. Park, *J. Cryst. Growth* 235, 572 (2002).
13. H. Yasuda, N. Notake, K. Tokeida, and I. Ohnaka, *J. Cryst. Growth* 210, 637 (2000).
14. P. Busse and F. Meissen, *Scripta Metall.* 36, 653 (1997).
15. T.B. Massalski, *Binary Alloy Phase Diagram* (Metals Park, OH: American Society for Metals, 1986), p. 235.
16. M.C. Flemings, *Solidification Processing* (NewYork: McGraw Hill, 1974), pp. 31–53.
17. T.S. Lo, S. Dobler, M. Plapp, A. Karma, and W. Kurz, *Acta Metall.* 51, 599 (2003).
18. M. Gündüz, H. Kaya, E. Çadırlı, N. Maraşlı, K. Keşlioğlu, and B. Saatçi, *J. Alloys Compd.* 439, 114 (2007).
19. S. Ganesan, C.L. Chan, and D.R. Poirier, *Mater. Sci. Eng. A* 151, 97 (1992).
20. M.S. Bhat, D.R. Poirier, and J.C. Heinrich, *Met. Trans. B* 26, 1049 (1995).
21. P. Robinson, *Practical Specific Heat Determination by Power Compensation DSC* (UK: PerkinElmer Seer Green, 2003), p. 12.
22. Y. Kaygısız, S. Akbulut, Y. Ocak, K. Keşlioğlu, N. Maraşlı, E. Çadırlı, and H. Kaya, *J. Alloys Compd.* 487, 103 (2009).
23. H. Kaya, E. Çadırlı, U. Böyük, and N. Maraşlı, *Appl. Surf. Sci.* 255, 3071 (2008).
24. S. Khan, A. Ourdjini, Q.S. Hamed, M.A.A. Najafabadi, and R. Elliott, *J. Mater. Sci.* 28, 5957 (1993).
25. H. Kaya, M. Gündüz, E. Çadırlı, and O. Uzun, *J. Mater. Sci.* 39, 6571 (2004).

26. F. Vnuk, M. Sahoo, D. Baragor, and R.W. Smith, *J. Mater. Sci.* 15, 2573 (1980).
27. A.I. Telli and S.E. Kısakürek, *Mater. Sci. Technol.* 4, 153 (1988).
28. J. Lapin, L. Ondrus, and M. Nazmy, *Intermetallics* 10, 1019 (2002).
29. T. El-Ashram and R.M. Shalaby, *J. Electron. Mater.* 34, 212 (2005).
30. B. Saatci, M. Ari, M. Gündüz, F. Meydaneri, M. Bozoklu, and S. Durmus, *J. Phys.: Condens. Matter* 18, 10643 (2006).
31. C. Kittel, *Introduction to Solid State Physics*, 6th ed. (New York: Wiley, 1965), pp. 150–153.
32. R. Hultgren, R.L. Orr, P.D. Anderson, and K.K. Kelley, *Selected Values of Thermodynamic Properties of Metals and Alloys* (University of California, Berkeley: Wiley, 1963), pp. 318–322.